



NRC Publications Archive Archives des publications du CNRC

Carbon dioxide-induced crystallization in poly(L-lactic acid) and its effect on foam morphologies

Liao, Xia; Nawaby, Arghavan Victoria; Whitfield, Pamela S.

This publication could be one of several versions: author's original, accepted manuscript or the publisher's version. / La version de cette publication peut être l'une des suivantes : la version prépublication de l'auteur, la version acceptée du manuscrit ou la version de l'éditeur.

For the publisher's version, please access the DOI link below. / Pour consulter la version de l'éditeur, utilisez le lien DOI ci-dessous.

Publisher's version / Version de l'éditeur:

<https://doi.org/10.1002/pi.2910>

Polymer international, 59, 12, pp. 1709-1718, 2010-12-01

NRC Publications Record / Notice d'Archives des publications de CNRC:

<https://nrc-publications.canada.ca/eng/view/object/?id=d65db456-0881-45f7-991f-de42d7dd0bcb>

<https://publications-cnrc.canada.ca/fra/voir/objet/?id=d65db456-0881-45f7-991f-de42d7dd0bcb>

Access and use of this website and the material on it are subject to the Terms and Conditions set forth at

<https://nrc-publications.canada.ca/eng/copyright>

READ THESE TERMS AND CONDITIONS CAREFULLY BEFORE USING THIS WEBSITE.

L'accès à ce site Web et l'utilisation de son contenu sont assujettis aux conditions présentées dans le site

<https://publications-cnrc.canada.ca/fra/droits>

LISEZ CES CONDITIONS ATTENTIVEMENT AVANT D'UTILISER CE SITE WEB.

Questions? Contact the NRC Publications Archive team at

PublicationsArchive-ArchivesPublications@nrc-cnrc.gc.ca. If you wish to email the authors directly, please see the first page of the publication for their contact information.

Vous avez des questions? Nous pouvons vous aider. Pour communiquer directement avec un auteur, consultez la première page de la revue dans laquelle son article a été publié afin de trouver ses coordonnées. Si vous n'arrivez pas à les repérer, communiquez avec nous à PublicationsArchive-ArchivesPublications@nrc-cnrc.gc.ca.



Carbon dioxide-induced crystallization in poly(L-lactic acid) and its effect on foam morphologies

Xia Liao,* Arghavan Victoria Nawaby[†] and Pamela S Whitfield

Abstract

The effect of carbon dioxide (CO₂) on the physical properties of poly(L-lactic acid) (PLLA) and on the formation of crystalline domains was investigated. The presence of CO₂ in the matrix was found to induce crystallization in PLLA, with the crystallinity increasing with increasing CO₂ pressure. The combination of saturation conditions and formation of crystalline domains was studied for its effect on the formation of porous morphologies in PLLA. Moreover, the effect of CO₂ on PLLA properties and formation of porous structures was further exploited by first creating crystalline domains in samples using CO₂ at various pressures at 25 °C and then re-saturating the same samples with CO₂ at a constant pressure of 2.8 MPa and 0 °C. This paper reports on the solubility of CO₂ at 25 and 0 °C in PLLA, crystallization and subsequent effect on foam morphologies when processed using different saturation cycles. Unique and intriguing morphologies were obtained by specifically controlling the properties of PLLA.

Copyright © 2010 Crown in the right of Canada. Published by John Wiley & Sons, Ltd

Keywords: CO₂; poly(L-lactic acid); crystallization; foam morphology

INTRODUCTION

Using compressed carbon dioxide (CO₂) as a physical blowing agent to prepare polymer microcellular foams has received significant attention.^{1–5} The morphologies generated via CO₂ processing are dependent on treatment pressures and temperatures, the physical properties of the polymer and the modifications thus induced as a result of contact with CO₂. The solubility of CO₂ in a polymer leads to relaxation, chain mobility and hence reduction in the polymer's glass transition temperature (T_g). Sufficient relaxation in polymers caused either by heating or dissolution of CO₂ can result in an increase of free volume and hence chain ordering and crystallization in the polymers. CO₂-induced crystallization has been observed in poly(ethylene terephthalate) (PET),⁶ poly(*p*-phenylene sulfide),⁷ polycarbonate,⁸ poly(ether ether ketone),⁹ methyl-substituted poly(ether ether ketone)¹⁰ and poly(lactic acid) (PLA).¹¹ Under a CO₂ environment, the crystalline melt point (T_m) and cold crystallization temperature (T_c) are also depressed.^{10,12,13}

To date CO₂ foaming has been mainly applied to amorphous polymers. The foaming process of a semicrystalline polymer is much more complex than that of an amorphous polymer due to the presence of non-plasticized crystals. Studies have shown that the foaming processes of amorphous and semicrystalline polymers are significantly different.¹⁴ Polymers with a low degree of crystallinity produce an almost uniform porous structure. Interaction of a gas such as CO₂ has been demonstrated to increase the crystalline content and hence increase the pore density while decreasing the pore size.^{15,16} Semicrystalline polymers exhibit considerably higher pore densities than amorphous polymers as the crystalline domains may act as heterogeneous nucleation sites and heterogeneous nucleation may occur at the amorphous/crystalline interfacial regions.^{17,18} The crystalline

content of polymers controls the chain stiffness and a reduction in average pore size is observed in foamed samples as a function of crystallinity.¹⁷ With further increase in the crystallinity, a polymer shows difficulty in foaming, which is related to the highly ordered crystalline structure. The effects of crystallinity and its contribution to porous structure have been reported in syndiotactic polystyrene,¹⁴ polypropylene (PP),¹⁶ PET,^{16–19} high-density polyethylene (HDPE),¹⁶ polybutylene,¹⁶ poly(ester-amide),²⁰ HDPE/PP,²¹ HDPE/iPP²² and ω -pentadecalactone/ ϵ -caprolactone copolymer.²³ Smaller pore sizes and higher pore densities were achieved when samples were processed with CO₂.

Although detailed investigations are available on the effect of CO₂ on a wide range of petrochemical-based polymers and the processing of porous morphologies, data for the interaction of CO₂ with biopolymers are comparatively very limited. Using CO₂ to prepare biodegradable polymer foams has been done for poly(lactic-co-glycolic acid),^{24–26} poly(ϵ -caprolactone),^{27,28} poly(L-lactic acid) (PLLA),^{11,26,27} poly(glycolic acid),^{26,27} PLA,²⁹ PLA/silk composites³⁰ and PLA/layered silicate nanocomposites.^{31,32} Studies have also demonstrated that CO₂ is able to depress T_g and T_m ,^{33,34} and induce crystallization¹¹ in PLLA. The type of morphologies produced by CO₂ not only depends on the degree of solubility and temperatures at which instability

* Correspondence to: Xia Liao, College of Polymer Science and Engineering, Sichuan University, Chengdu 610065 China. E-mail: xliao@scu.edu.cn

[†] Present address: Sealed Air Corporation, 2401 Dillard Street, Grand Prairie, TX 75051, USA.

Institute for Chemical Process and Environmental Technology, National Research Council of Canada, Ottawa, Ontario K1A 0R6, Canada

Table 1. The crystallinity and crystal size of PLLA samples conditioned with CO₂ in 24 h cycles

Sample	Procedure	Crystallinity (%)	Crystallite size (nm)
PLLA1	Saturated with CO ₂ at 25 °C, 0.1 MPa, pressure quenched, and then re-saturated with CO ₂ at 0 °C, 2.8 MPa	12	2.3 ± 0.6
PLLA2	Saturated with CO ₂ at 25 °C, 1.4 MPa, pressure quenched, and then re-saturated with CO ₂ at 0 °C, 2.8 MPa	14	2.2 ± 0.6
PLLA3	Saturated with CO ₂ at 25 °C, 2.1 MPa, pressure quenched, and then re-saturated with CO ₂ at 0 °C, 2.8 MPa	15	4.1
PLLA4	Saturated with CO ₂ at 25 °C, 2.8 MPa, pressure quenched, and then re-saturated with CO ₂ at 0 °C, 2.8 MPa	20	7.4
PLLA5	Saturated with CO ₂ at 25 °C, 3.5 MPa, pressure quenched, and then re-saturated with CO ₂ at 0 °C, 2.8 MPa	30	12.7

in the system is established, but also on the physical properties of polymers. The crystallization induced by dissolution of CO₂ in PLLA during foam processing results in porous morphologies vastly different from the pore morphologies expected of the amorphous material.¹¹

Although CO₂-induced crystallization has been well studied, there is still a lack of understanding of the effect of crystallization on PLLA foam morphology. The purpose of the present paper is, therefore, to report on CO₂-induced crystallization in PLLA and its role in the resultant unique foam morphologies.

EXPERIMENTAL

Materials

PLLA pellets (weight-average molecular weight $M_w = 58\,000\text{ g mol}^{-1}$, $M_w/M_n = 1.7$, density = 1.24 g cm^{-3} , $T_g = 54\text{ °C}$, $T_c = 83\text{ °C}$ and $T_m = 170\text{ °C}$) were supplied by Birmingham Polymer Inc. Bone-dry 99% pure CO₂ was used. PLLA samples in sheets 300–400 μm thick were prepared by compression molding at 190 °C followed by quenching in ice water.

Gas solubility measurements

Sorption kinetic studies were carried out using a Cahn D110 microbalance.³⁵ Polymer samples were placed in the balance and evacuated for 48 h. CO₂ gas was added in small pressure steps while the weight change as a function of time was recorded every 10 s until equilibrium for each pressure step was established. Sorption studies for a desired pressure range in this manner were carried out at 25 and 0 °C. Blank runs were also carried out under similar experimental conditions and solubility data were corrected for balance zero shift. Since sorption of gases in polymers causes dilation, all sorption runs were corrected for buoyancy effects. Diffusion coefficients of CO₂ in PLLA were then estimated from the sorption curves using a hybrid model.

CO₂-induced crystallization

The effect of CO₂ on the crystallization of PLLA at various gas pressures was investigated using a Bruker GADDS diffraction system with Co K_α and a two-dimensional HISTAR detector. Samples prior to contact with CO₂ and samples treated with CO₂ under various saturation conditions were analyzed. After saturation at various pressures and temperatures for various time intervals, the pressure in the vessel was released rapidly and samples were aged for at least 5 days prior to obtaining XRD patterns. Samples were analyzed in transmission mode with a 1 mm monocapillary optic and a collimator-mounted beamstop. The background scatter was subtracted from the collected frames after accounting for the attenuation of the scattering by the sample using $I/I_0 = t \exp(-\mu t)$, where t is the sample thickness and μ

is the linear absorption coefficient. The background-corrected frames were then analyzed using the rolling-ball algorithm in the Bruker GADDS software to separate the crystalline and amorphous fractions.

The instrument function of the particular configuration was obtained by collecting data from a thin layer of SRM660a LaB₆ line profile standard sprinkled onto tape and analyzed in transmission. The line profiles were modeled in Topas 3, and the effective column length determined by convoluting a Lorentzian function into the instrument function with a $1/\cos \theta$ angular dependence. Errors in the form of estimated standard deviations were determined for the size measurements.

Foaming and foam characterization

Amorphous test samples were prepared by compression molding at 190 °C followed by quenching in ice water. Foamed specimens were prepared by saturating PLLA samples with CO₂ at 25 °C and various pressures from 1.4 to 5.5 MPa for various saturation times.

PLLA samples of various crystallinities were prepared by saturating the specimens with CO₂ at pressures of 0.1, 1.4, 2.1, 2.8 and 3.5 MPa at 25 °C for 24 h (first saturation cycle). Each PLLA sample was then aged for at least 7 days prior to being further saturated with CO₂ at 2.8 MPa and 0 °C for 24 h with each individual sample being designated as PLLA1, PLLA2, PLLA3, PLLA4 and PLLA5 (second saturation cycle). The saturation conditions are presented in Table 1. Following the second saturation cycle the PLLA1, PLLA2, PLLA3, PLLA4 and PLLA5 samples were rapidly depressurized and subsequently foamed at temperatures between 50 and 100 °C.

Foam morphologies were analyzed using SEM with JEOL JSM 840A and Hitachi S4800 field emission instruments. The foam density was measured by weighing samples in air and in water using an electronic balance with a resolution of ±10 μg.

RESULTS AND DISCUSSION

CO₂-induced crystallization

It is known that absorbed CO₂ in a polymer reduces T_g of the polymer due to the increase in the free volume fraction that enhances the mobility of polymer chains. The absorption of CO₂ results in considerable swelling in amorphous polymers and crystallization in semicrystalline polymers by reordering polymer chains at lower temperatures.^{7,8,13,36} Figure 1 shows the XRD patterns for the untreated sample and the samples saturated with CO₂ at 1.4, 2.1, 2.8, 3.5 and 5.5 MPa and 25 °C for 24 h. The untreated sample is amorphous as evident from the XRD analysis. Obviously, the presence of CO₂ does not change the crystalline structure of PLLA and the diffraction peaks become narrower and more intense with increasing pressure. The values

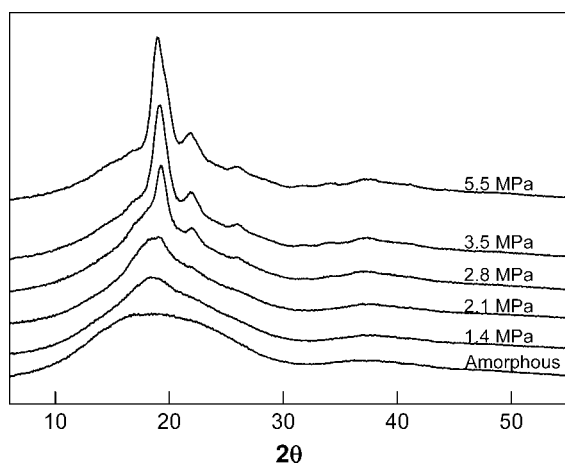


Figure 1. XRD patterns for the PLLA–CO₂ system as a function of pressure (samples saturated at 25 °C with a contact time of 24 h).

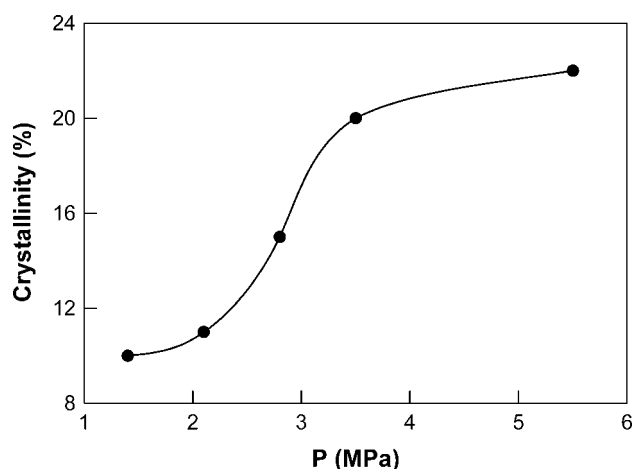


Figure 2. Pressure dependence CO₂-induced crystallinity (samples saturated at 25 °C with a contact time of 24 h).

of crystallinity derived from the XRD patterns are shown in Fig. 2, which indicates the crystallinity increases with increasing pressure. As the CO₂ pressure is increased, the volume fraction of CO₂ absorbed by the samples increases, thus enhancing chain mobility and lowering T_g at the same time. Therefore, the realignment of the chains to a crystalline structure of lower free energy is thermodynamically favorable, resulting in higher crystallinity at elevated pressure.

Solubility and diffusion coefficient

The sorption kinetics of CO₂ in PLLA was investigated by recording the changes of gas uptake in the polymer over time until a stable value was obtained. In amorphous polymer, CO₂ diffuses into the whole polymer matrix. A typical sorption curve of CO₂ in amorphous polymer shows an increase in solubility with increasing saturation time which then levels off when equilibrium is achieved. The crystalline domains generated by contacting CO₂ in semicrystalline polymers complicate the CO₂ diffusion process. The sorption curves of CO₂ in PLLA at 25 °C above 1.4 MPa exhibit a distinctive kink which demonstrates that CO₂ induces crystallization and the crystal regions reject CO₂.¹¹ Since the gas does not diffuse through the crystalline regions

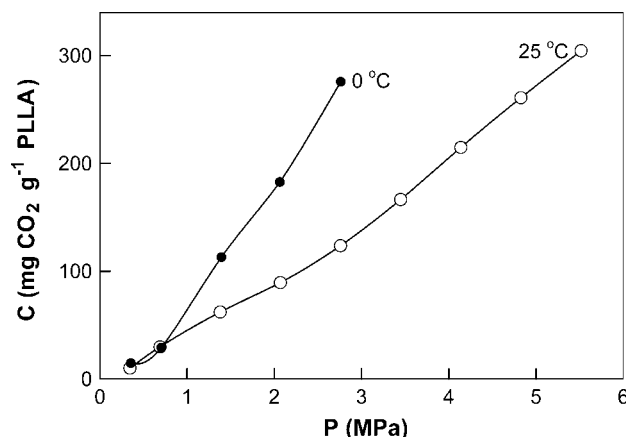


Figure 3. Solubility of CO₂ in PLLA as a function of pressure at 0 and 25 °C.

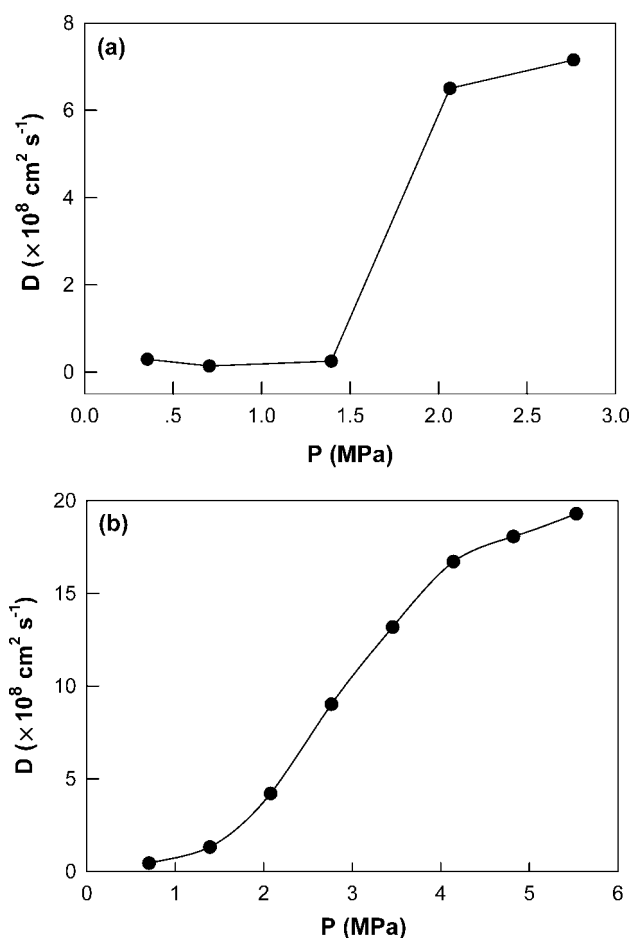


Figure 4. Diffusion coefficient (D) of CO₂ in PLLA at (a) 0 °C and (b) 25 °C.

and the crystalline phase does not absorb gas, the equilibrium solubility and diffusion coefficient data in semicrystalline polymers are corrected from the unit weight of the amorphous regions.¹⁹

The solubilities of CO₂ in PLLA at 0 and 25 °C and an equilibrium pressure up to 2.8 and 5.5 MPa, respectively, are shown in Fig. 3. The solubility increases with increasing pressure. The gas uptake at 5.5 MPa after correction for crystallinity content

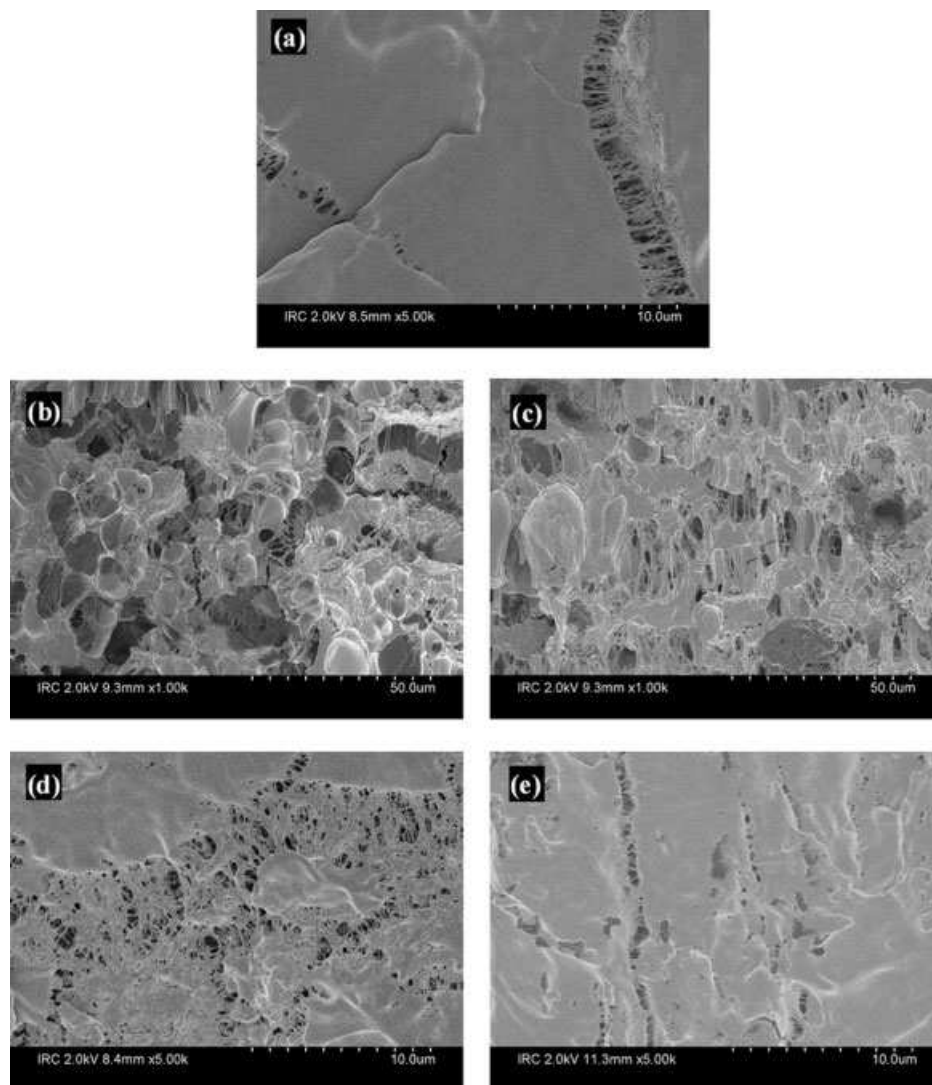


Figure 5. SEM micrographs of PLLA foams as a function of saturation pressure: (a) 2.1 MPa; (b) 2.8 MPa; (c) 3.5 MPa; (d) 4.1 MPa; (e) 5.5 MPa. (Samples saturated at 25 °C for 24 h and subsequently foamed at 90 °C).

is about 300 mg g⁻¹ PLLA, which is higher than the solubility of CO₂ in poly(methyl methacrylate) (230 mg g⁻¹) for the same experimental conditions.³⁷ It has been reported that polymers such as poly(methyl methacrylate) possessing electron-donating functional (e.g. carbonyl) groups present higher CO₂ solubility than other polymers such as polystyrene and polyethylene, which is due to the specific intermolecular interactions between CO₂ and the electron-donating functional groups, in the form of an electron donor–acceptor complex.^{38,39} Such specific interactions were also detected for CO₂ with poly(butyl methacrylate) and poly(ethyl methacrylate) which contain Lewis base groups. Koros reported that CO₂ solubility increases with the density of carbonyl groups in the polymer.⁴⁰ Therefore, the high solubility of CO₂ in PLLA is probably due to the specific interactions of CO₂ with the carbonyl groups in PLLA.

Diffusion coefficients at various pressures and temperatures were obtained by fitting the sorption kinetic data to a hybrid model, as shown in Fig. 4. The diffusion coefficient increases with increasing pressure. The increase in diffusion coefficient is attributed to the high degree of plasticization in the amorphous phase as a result of higher gas solubility with increasing pressure.

Effect of pressure and saturation time on pore morphology

The solubility of CO₂ in polymers is controlled by changing the saturation conditions such as temperature and pressure, which can be utilized to adjust the amount of available foaming agent to further control pore morphology. Figure 5 shows SEM micrographs of samples saturated at 25 °C and various CO₂ pressure for 24 h and subsequently foamed at 90 °C for 30 s. PLLA saturated at 2.1 MPa exhibits a non-uniform layered morphology with partially interconnected pores (Fig. 5(a)). More uniform partially open pore structure is obtained for saturation at 2.8 MPa (Fig. 5(b)). With an increase in pressure to 3.5 MPa, the foam obtained shows a decrease in pore diameter (Fig. 5(c)). As observed in Fig. 3, the solubility increases with increasing pressure. For amorphous polymers, the pore density and pore structure are dependent on the amount of gas dissolved in the matrix when other conditions are similar. An increase in the amount of dissolved gas with increasing pressure can induce a larger pore density during the foaming process. However, for saturation pressure above 3.5 MPa, the samples exhibit foaming difficulties. The foamed PLLA sample shows an uneven structure with small pore diameter at 4.1 MPa

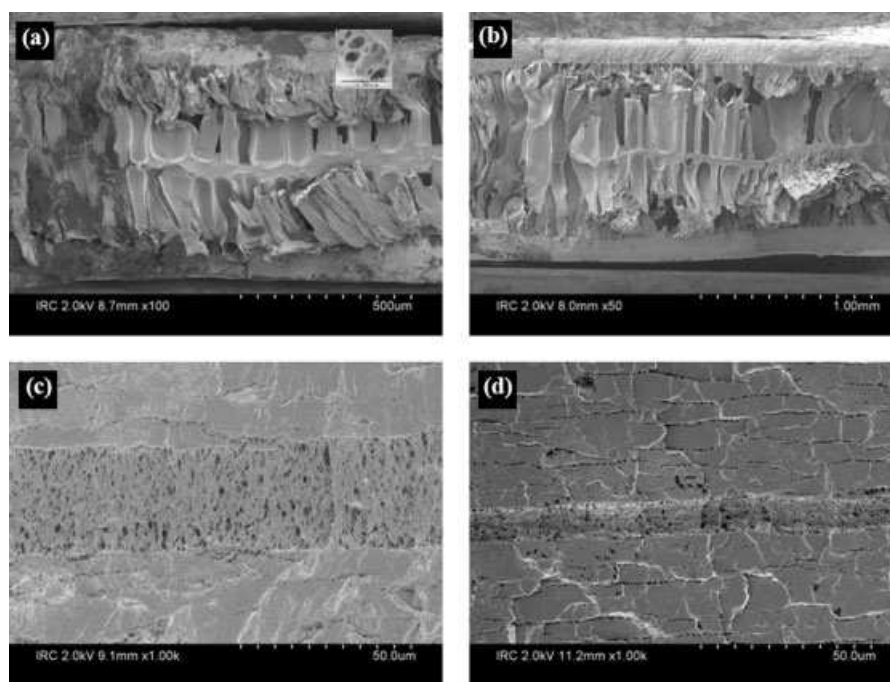


Figure 6. SEM micrographs of PLLA foams as a function of contact time: (a) 3 min; (b) 5 min; (c) 10 min; (d) 24 h. (Samples saturated at 25 °C and 5.5 MPa, and subsequently foamed at 60 °C).

(Fig. 5(d)). On increasing the pressure to 5.5 MPa, the foamed sample has a layered pore structure (Fig. 5(e)).

Since CO₂ does not dissolve in the crystalline regions, compared with amorphous polymers it is more difficult to use semicrystalline polymers in the foaming process. However, crystallized PET shows small pore sizes and large pore densities on using CO₂ as a foaming agent.^{17–19} The CO₂-induced crystallinity in PET is the dominant factor affecting pore nucleation and growth in PET foams. An increase in saturation pressure in amorphous polymers causes a decrease in the free energy barrier for the formation of stable nuclei and the activation of additional nucleation sites due to matrix swelling and free volume changes, thus resulting in larger pore nucleation sites and a higher pore density.¹⁷ In the PLLA–CO₂ system, the crystallinity induced by CO₂ can be an additional important factor in the foaming process as observed in the PET–CO₂ system. Although the solubility of CO₂ in PLLA increases with increasing pressure, the sample saturated at a pressure above 3.5 MPa showed foaming difficulties. XRD data (Fig. 2) for PLLA samples saturated at 25 °C reveal an increase in crystallinity with increasing saturation pressure. The difference in the resulting porous structures of PLLA samples is probably due to the different crystallinity induced by CO₂ at various pressures.

To further investigate the role of crystallinity in the foam morphology, PLLA samples were saturated at 25 °C and 5.5 MPa for various periods of time and subsequently foamed at 60 °C. Unlike the typical foam structure of polymers processed with CO₂ producing a porous core and an apparently nonporous skin, PLLA saturated for 3 min (Fig. 6(a)) shows a unique core–skin structure with a partially open nanopore structure in the skin. As postulated by Kumar and Wells,⁴¹ the formation of a nonporous skin in the foaming process is attributed to gas molecules near the edges of the samples diffusing out of the sample faster than they can join nuclei. Rapid diffusion out of the sample creates a depletion layer near the edges where the CO₂ concentration is too low to significantly participate in bubble nucleation and growth. The

core–skin structure observed in PLLA therefore can be attributed to the high solubility of CO₂ in PLLA, which provides enough gas for pore nucleation and growth in the skin. Moreover, since the saturation time is too short to allow CO₂ to completely diffuse into the center of the sample according to the diffusion coefficient data (Fig. 4), a partially unfoamed area in the middle of the sample is observed (Fig. 6(a)). On increasing the saturation time to 5 min, uniform core–skin morphology is obtained (Fig. 6(b)). However, with an increase in saturation time to 10 min, the core–skin structure with large stretched pores in the core and partially open and interconnected pores in the skin disappears, and instead a foamed core with pore size in the range 50–600 nm and layered foam towards the surface are observed (Fig. 6(c)). XRD analysis of PLLA samples saturated at 5.5 MPa reveals an increase in crystallinity with increasing saturation time which then levels off (Fig. 7). Such results indicate that there is a critical level of crystallinity to result in foaming difficulties. The reduced pore size of the sample saturated for 10 min is mostly because of the increased matrix stiffness associated with crystallization. A fine layered interconnected foam structure with partially open pores in the size range 200–500 nm within the layers is obtained when PLLA is saturated with CO₂ at 5.5 MPa for 1 day and foamed at 60 °C (Fig. 6(d)). The results clearly show that the crystallization process plays a vital role in forming porous PLLA morphologies.

The crystallinity and solubility of CO₂ in PLLA both depend on saturation pressure or saturation time. In order to further investigate the effects of crystallinity on the foam processing and foam morphologies, five PLLA samples with various crystallinities were prepared.

Effect of crystallinity on foam morphology

PLLA samples with various crystallinities were prepared by saturating the specimens with CO₂ gas under various saturation conditions. The details are listed in Table 1. The XRD patterns are

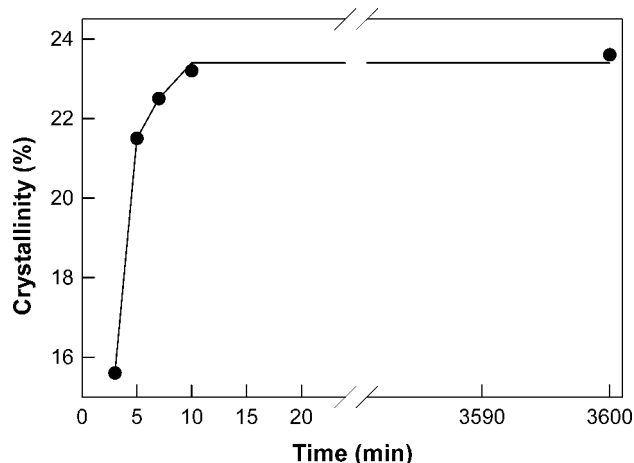


Figure 7. CO₂-induced crystallization in PLLA as a function of contact time (sample saturated at 25 °C and 5.5 MPa).

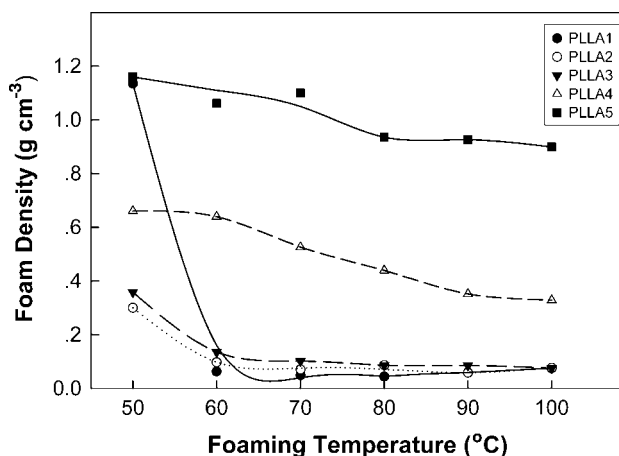


Figure 9. Foam density as a function of foaming temperature.

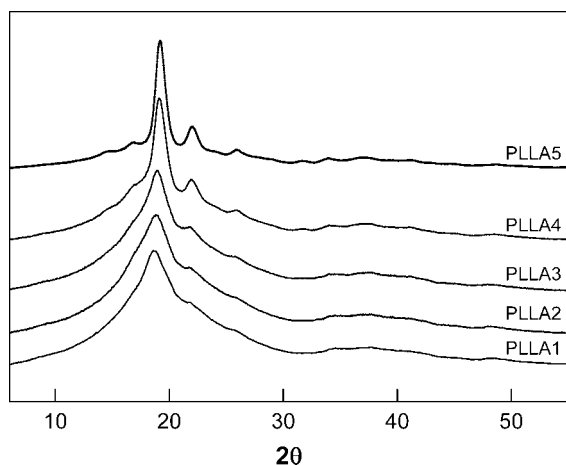


Figure 8. XRD patterns of PLLA samples prepared in CO₂ under various saturation conditions.

shown in Fig. 8 and the crystallinity data and crystallite sizes are presented in Table 1.

To investigate the effect of crystallinity on the foaming behavior, PLLA samples (PLLA1, PLLA2, PLLA3, PLLA4 and PLLA5) with various crystallinities were foamed in the temperature range 50–100 °C. The foam densities obtained as a function of foaming temperatures are shown in Fig. 9 for each of the five samples investigated. It is interesting to note that the foam density of PLLA1 obtained at 50 °C is 1.14 g cm⁻³ which is close to that of the neat polymer (1.24 g cm⁻³). Meanwhile, the foam densities obtained at 50 °C for PLLA2, PLLA3, PLLA4 and PLLA5 are 0.30, 0.36, 0.66 and 1.16 g cm⁻³, respectively. In the case of PLLA2, PLLA3 and PLLA4, the pore nucleation and growth is noted to occur at lower temperatures. However, when the crystallinity is higher than 20% (PLLA5) no improvement occurs in the foam density with increasing foaming temperature when compared with the other PLLA samples. The lack of foaming of highly crystalline polymers is likely to be related to the highly ordered crystalline structure, which increases the polymer modulus by several orders of magnitude.

The pore morphology and properties of a foaming material are controlled by the pore nucleation and pore growth processes.

Since the sorption of gases in semicrystalline polymers occurs exclusively in the amorphous regions, CO₂ solubility and diffusion coefficient in the amorphous phase of the PLLA samples (PLLA1, PLLA2, PLLA3, PLLA4 and PLLA5) with various crystallinities are considered as the same. Therefore, the different pore morphologies of PLLA samples with various crystallinities processed under the same conditions can probably be attributed to the different behaviors of pore nucleation and pore growth.

Pore nucleation is the formation of a new gas phase from a metastable phase, which requires an activation energy barrier to be overcome to generate phase separation. Pore nucleation may occur homogeneously throughout the matrix or heterogeneously at some high-energy regions such as microvoids and phase interfaces. The activation energy to develop a stable bubble in such regions is lower than in other regions, which leads to preferential nucleation of pores at the interface. Figure 10 shows SEM micrographs of foams obtained for the PLLA samples with various degrees of crystallinity foamed at 50 °C. PLLA1 which has the lowest crystallinity only shows a few foamed layers (Fig. 10(a)). However, at a foaming temperature of 60 °C, the foam density of PLLA1 (0.06 g cm⁻³) decreases dramatically (Fig. 9), indicating that upon formation of the nuclei the pores grow rapidly. Baldwin *et al.*^{17–19} in their work on the foaming of PET suggested that the interfaces between crystalline and amorphous regions might be the preferential nucleation sites of microbubbles during the foaming process. The lack of foam in PLLA1 at 50 °C is probably due to the absence of available nucleating sites such as crystallites and amorphous–crystalline interfaces. With an increase in crystallinity, the free energy barrier for forming stable nuclei decreases due to there being more crystalline interfaces. More importantly, the number of potential nucleation sites increases with increasing crystallinity. Therefore, PLLA2 and PLLA3 foams obtained at 50 °C exhibit pore morphologies that are partially interconnected (Figs 10(b) and (c)). Since CO₂ gas does not dissolve in the crystallites, the nucleation is non-homogeneous. This leads to the difficulties in controlling the porous morphology of polymers with a high degree of crystallinity. Consequently, PLLA4 with a crystallinity of 20% produces a non-uniform foamed structure (Fig. 10(d)) indicating a maximum limit in crystallinity in order to obtain a homogeneous porous structure. With a further increase in crystallinity to 30%, PLLA5 does not show any detectable pore structures. It has been reported that crystallization resulting in a semicrystalline polymer requires relatively high temperatures

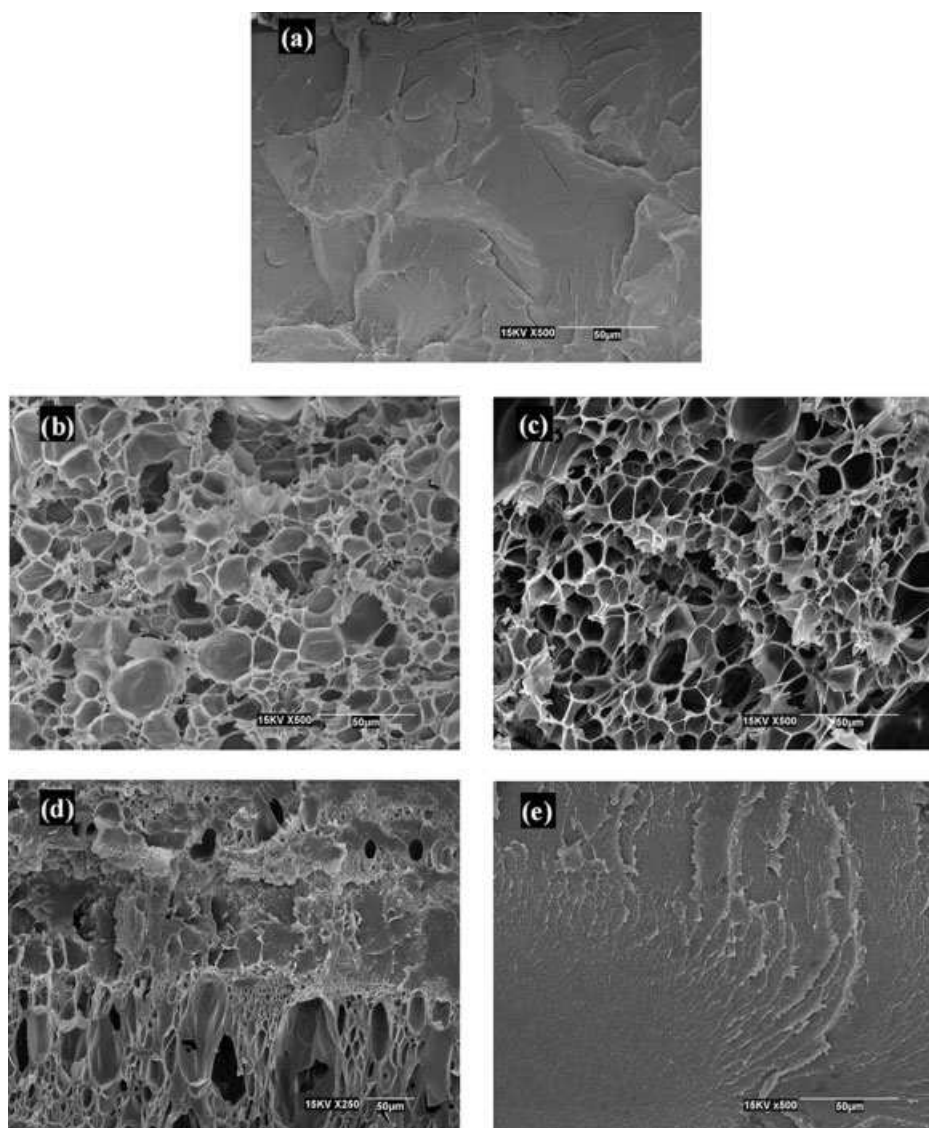


Figure 10. SEM micrographs of CO₂-foamed samples: (a) PLLA1; (b) PLLA2; (c) PLLA3; (d) PLLA4; (e) PLLA5. (Samples foamed at 50 °C).

for obtaining pore morphologies compared with an amorphous polymer–gas system.¹⁹ Since the stiffness of the polymer chains affects the foamed structure significantly during the foaming process, the lack of detectable pore structures at the lower foaming temperatures in higher crystallinity PLLA (PLLA5) could be attributed to the pore growth behavior of semicrystalline polymers.

Normally, pore growth is governed by the rate of gas diffusion into the pores, the time allowed for gas to diffuse into the pores before quenching, the temperature of the foaming system, the degree of supersaturation and the viscoelastic properties of the polymer–gas mixture.^{17–19} When the foaming conditions such as time, temperature, degree of supersaturation and gas diffusion in the amorphous phase of PLLA samples are similar, the pore growth depends on the viscoelastic behavior of the matrix. The stiffness of the polymer matrix is controlled by the crystallinity and increases with increasing crystallinity.¹⁶ SEM micrographs of foams obtained for PLLA with various degrees of crystallinity at 70 °C are shown in Fig. 11. PLLA1, PLLA2 and PLLA3 with lower crystallinity are more softened because they have more amorphous regions, which

exhibit uniform partially interconnected pore morphologies as shown in Figs 11(a)–(c), respectively. PLLA4 with a crystallinity of 20% shows non-uniform foamed morphology and does not exhibit fully grown pore structures in the middle (Fig. 11(d)). PLLA5 which has 30% crystallinity produces only some gaps (Fig. 11(e)). The foaming difficulties apparent for highly crystalline polymers are likely related to the highly ordered crystalline domains, which enhance the modulus of polymer chains by several orders of magnitude.¹⁹ In this case, the primary factor affecting pore growth is the temperature-dependent relaxation modulus.

Increasing the foaming temperature leads to a decrease in the viscosity of the polymer matrix and to an increase in the supersaturation of the polymer–gas system. In semicrystalline polymers, the pore growth is controlled by the viscoelastic behavior of the matrix. The foaming temperature can affect the gas diffusion rate, the interfacial surface energy and the viscosity of the polymer–gas matrix thus controlling the pore growth. Therefore the foaming temperature is an important processing parameter which controls the foam morphology. Larger pores are obtained (Fig. 12) when samples are foamed at 80 °C compared

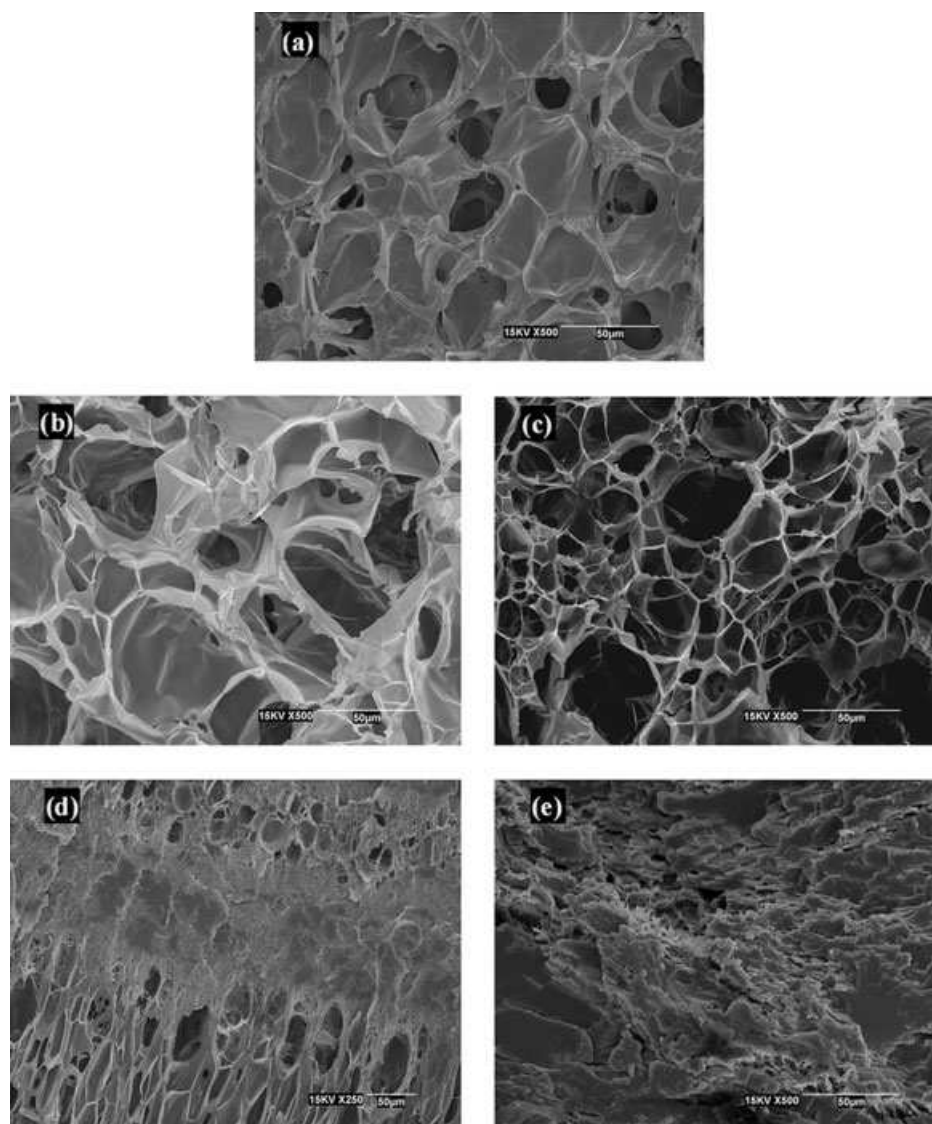


Figure 11. SEM micrographs of CO₂-foamed samples: (a) PLLA1; (b) PLLA2; (c) PLLA3; (d) PLLA4; (e) PLLA5. (Samples foamed at 70 °C).

with samples foamed at lower temperatures (Figs 10 and 11). Higher pore densities and smaller pore sizes are achieved with an increase in crystallinity. However, a maximum limiting crystallinity is observed, above which a porous structure is obtained. PLLA5 foamed at 80 °C shows only some discontinuous gaps (Fig. 12(e)).

It should be noted that PLLA4 foamed at 80 °C shows a unique foam morphology: large pores with pore diameters of 10–30 µm in the outer layer and interconnected nanopores in the inner layer (Fig. 12(d)). At foaming temperatures lower than 80 °C, the matrix stiffness may be too large to allow nucleated pores in the middle of the sample to grow into detectable sizes. Therefore, nucleation may have occurred in the low-temperature samples, but the growth of stable nuclei was not sufficient for them to be detected.

CONCLUSIONS

Solubility and diffusion coefficients of CO₂ in PLLA have been measured at 0 and 25 °C. Based upon XRD analysis it was found that CO₂ induces crystallinity in the samples with the degree of

crystallinity increasing with increasing saturation pressure and time. PLLA samples with various crystallinities were prepared by saturating with CO₂ at various gas pressures to investigate the effect of crystallinity on foam processing and foam morphology. The foam density, pore density and pore size are dependent on the crystallinity, pressure and temperature. The foam density of PLLA increases with increasing crystallinity and decreases with foaming temperature. Partially interconnected pore structures were obtained and the pores size increases with increasing foaming temperature. Higher pore densities and smaller pore sizes were achieved with increasing crystallinity. A limit on the crystal content of the samples, however, was found to affect the structure of the matrix. Various novel foam morphologies such as core–skin, layered and interconnected structures are obtained by tuning the crystallinity in PLLA induced by exposure to CO₂.

ACKNOWLEDGEMENTS

The authors thank Mr David Kingston and Mr James Margeson for their assistance with SEM work.

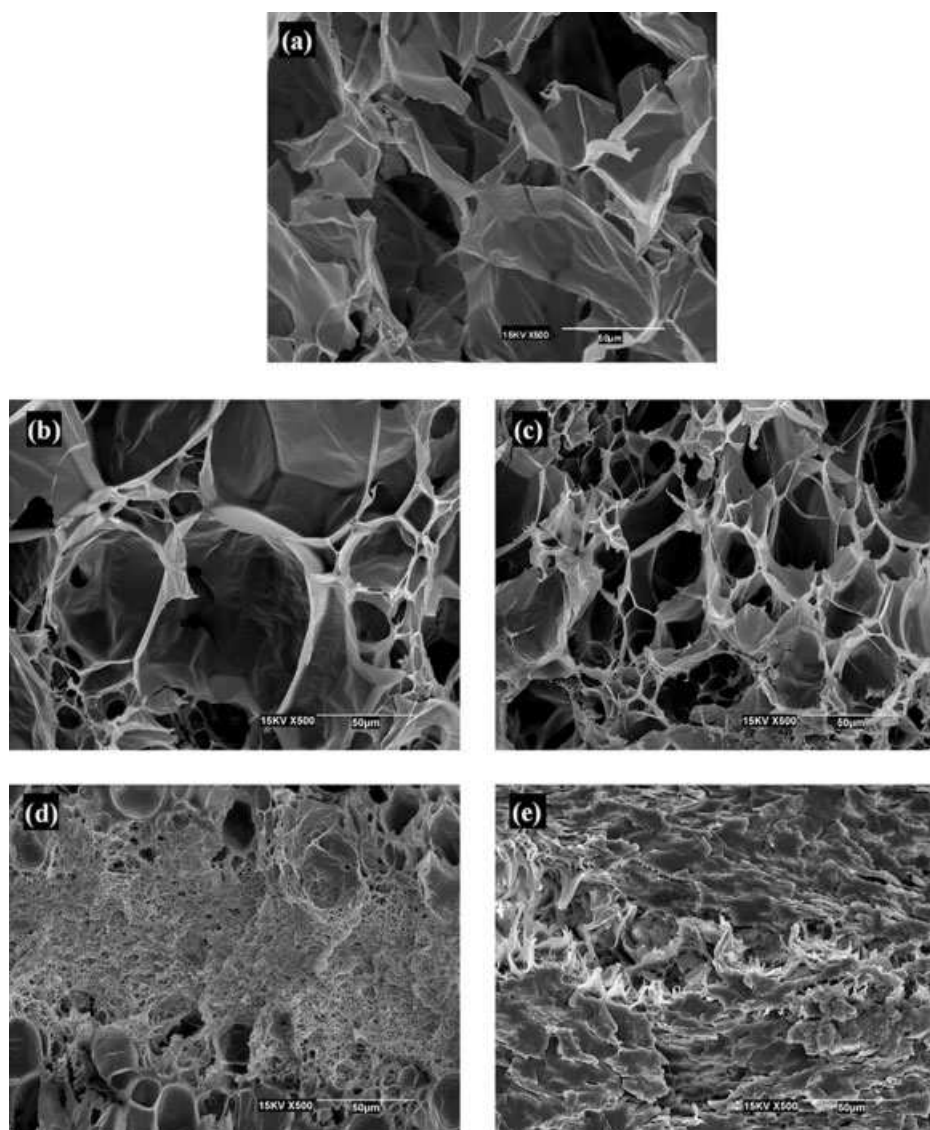


Figure 12. SEM micrographs of CO₂-foamed samples: (a) PLLA1; (b) PLLA2; (c) PLLA3; (d) PLLA4; (e) PLLA5. (Samples foamed at 80 °C).

REFERENCES

- Colton JS and Suh NP, *Polym Eng Sci* **27**:485–492 (1987).
- Goel SK and Beckman EJ, *Polym Eng Sci* **34**:1137–1147 (1994).
- Arora KA, Lesser AJ and McCarthy TJ, *Macromolecules* **31**:4614–4620 (1998).
- Zeng CC, Han XM, Lee LJ, Koelling, KW and Tomasko D, *Adv Mater* **15**:1743–1747 (2003).
- Nawaby AV, Handa YP, Liao X, Yoshitaka Y and Tomohiro M, *Polym Int* **56**:67–73 (2007).
- Mizoguchi K, Kirose T and Kamiya Y, *Polymer* **28**:1298–1302 (1987).
- Schultze JD, Engelman IAD, Boehning M and Springer J, *Polym Adv Technol* **2**:123–126 (1991).
- Handa YP and Porter RS, *J Polym Sci B: Polym Phys* **25**:1511–1517 (1987).
- Handa YP, Roovers J and Moulinié P, *J Polym Sci B: Polym Phys* **35**:2355–2362 (1997).
- Handa YP, Roovers J and Wang F, *Macromolecules* **27**:5511–5516 (1994).
- Liao X, Nawaby AV, Whitfield P, Day M, Champagne M and Denault J, *Biomacromolecules* **7**:2937–2941 (2006).
- Zhang Z, Nawaby AV and Day M, *J Polym Sci B: Polym Phys* **41**:1518–1525 (2003).
- Handa YP, Zhang Z and Wong B, *Macromolecules* **30**:8499–8504 (1997).
- Handa YP, Zhang Z, Nawaby V and Tan J, *Cellular Polym* **20**:241–253 (2001).
- Sha H and Harrison IR, *J Polym Sci B: Polym Phys* **30**:915–922 (1992).
- Doroudiani S, Park CB and Kortschot MT, *Polym Eng Sci* **36**:2645–2662 (1996).
- Baldwin DF, Park CB and Suh NP, *Polym Eng Sci* **36**:1437–1445 (1996).
- Baldwin DF, Park CB and Suh NP, *Polym Eng Sci* **36**:1446–1453 (1996).
- Baldwin DF, Shimbo M and Suh NP, *J Eng Mater Technol* **117**:62–74 (1995).
- Lips PAM, Velthoen IW, Dijkstra PJ, Wessling M and Feijen J, *Polymer* **46**:9396–9403 (2005).
- Rachtanapun P, Selke SEM and Matuana LM, *J Appl Polym Sci* **88**:2842–2850 (2003).
- Doroudiani S, Park CB and Kortschot MT, *Polym Eng Sci* **38**:1205–1215 (1998).
- Gualandi C, White LJ, Chen L, Gross RA, Shakesheff KM, Howdle SM, *et al*, *Acta Biomater* **6**:130–136 (2010).
- Singh L, Kumar V and Ratner BD, *Biomaterials* **25**:2611–2617 (2004).
- Mooney DJ, Baldwin DF, Suh NP, Vacanti JP and Langer R, *Biomaterials* **17**:1417–1422 (1996).
- Sheridan MH, Shea D, Peters MC and Mooney DJ, *J Controlled Release* **64**:91–102 (2000).
- Jenkins MJ, Harrison KL, Silva MCG, Whitaker MJ, Shakesheff KM and Howdle SM, *Eur Polym J* **42**:3145–3151 (2006).

- 28 Nawaby AV, Farah AA, Liao X, Pietro WJ and Day M, *Biomacromolecules* **6**:2458–2461 (2005).
- 29 Kang DJ, Xu D, Zhang ZX, Pal K, Bang DS and Kim JK, *Macromol Mater Eng* **294**:620–624 (2009).
- 30 Salerno A, Iannace S and Netti PA, *Macromol Biosci* **8**:655–664 (2008).
- 31 Fujimoto Y, Ray SS, Okamoto M, Ogami A, Yamada K and Ueda K, *Macromol Rapid Commun* **24**:457–461 (2003).
- 32 Ray SS and Okamoto M, *Macromol Mater Eng* **288**:936–944 (2003).
- 33 Sato Y, Yamane M, Sorakubo A, Takishima S, Masuoka H, Yamamoto H, *et al*, Proceedings of the 21st Japan Symposium on Thermophysical Properties, Nagoya, vol. B231, pp. 196–198 (2000).
- 34 Takada M, Hasegawa S and Ohshima M, *Polym Eng Sci* **44**:186–196 (2004).
- 35 Wong B, Zhang Z and Handa YP, *J Polym Sci B: Polym Phys* **36**:2025–2032 (1998).
- 36 Handa YP, Zhang Z and Roovers J, *J Polym Sci B: Polym Phys* **39**:1505–1512 (2001).
- 37 Handa YP, Zhang Z and Wong B, *Cellular Polym* **20**:1–16 (2001).
- 38 Kazarian SG, Vicent MF, Bright FV, Liotta CL and Eckert CA, *J Am Chem Soc* **118**:1729–1736 (1996).
- 39 Kazarian SG, *Macromol Symp* **184**:215–228 (2002).
- 40 Koros WJ, *J Polym Sci B: Polym Phys* **23**:1611–1628 (1985).
- 41 Kumar V and Wells JE, *SPE ANTEC Tech Papers* **38**:1508–1512 (1992).